Viscous and inviscid instabilities of supersonic flow in a streamwise corner

Oliver T. Schmidt and Ulrich Rist

Institut für Aerodynamik und Gasdynamik, Universität Stuttgart, 70550 Stuttgart, Germany

The linear stability of supersonic flow in a streamwise corner is examined. A steady base flow at a free-stream Mach number of $Ma = 1.5$ is calculated as a solution to the parabolized Navier-Stokes equations. Temporal growth rates for incoming and outgoing waves are compared. A new inviscid odd-symmetric corner mode not present in the incompressible spectrum is identified. Additionally, fast and slow traveling acoustic modes are calculated in an enlarged computational domain and categorized with respect to bisector-symmetry and wall-boundedness.

Nomenclature

α, β	streamwise and spanwise wave numbers
δ_1	displacement thickness
$\imath$	imaginary unit
κ	heat capacity ratio
Ma	Mach number
$\boldsymbol{\sigma}$	sponge zone weight function
$\mathbf{q}$	vector of primitive variables
A, B, C	PNS coefficient matrices
$\mathsf{D_y}$, $\mathsf{D_z}$	Chebyshev differentiation matrices
L, $\mathbf{r}$	linear PNS operator and right hand side
μ	dynamic viscosity
ω	angular frequency
ρ	density
a	speed of sound
a, b	grid transformation factors
c	phase speed
c_p, c_v	heat capacity at constant pressure and volume, respectively
k	thermal conductivity
N	number of collocation points
Pr	Prandtl number
R	ideal gas constant
Re_x	Reynolds number
T	temperature
u, v, w	Cartesian velocity components
x, y, z	Cartesian coordinates

I. Introduction

We consider the linear stability of shock-free compressible flow along an axial corner formed by two perpendicular semi-infinite flat plates. The generic corner flow problem is of major interest as it models a wide range of technical applications, e.g. the wing-fuselage or fin-fuselage intersections of an airplane. Figure 1 depicts a schematic diagram of the geometry. Here, x, y and z denote the streamwise coordinate and the two spanwise coordinates, respectively. At distances far from the corner, the flow resembles the two-

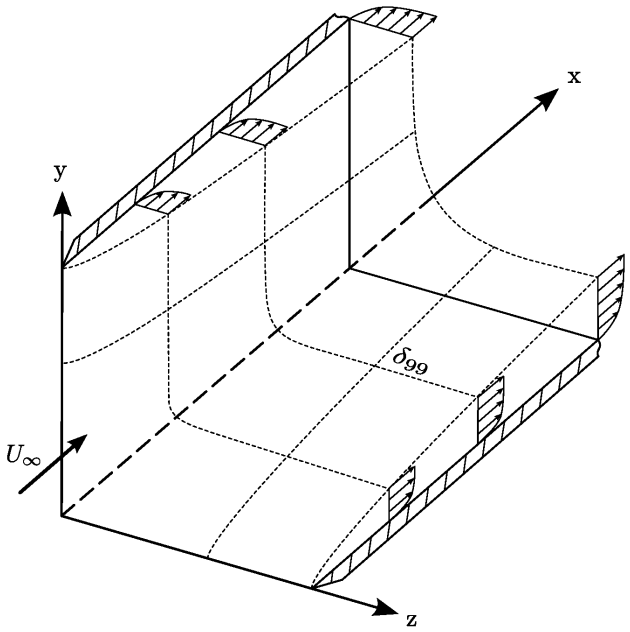

Figure 1. Schematic diagram of flow in a streamwise corner.

dimensional flow over a flat plate with an additional cross-flow velocity component caused by the displacement effect of the opposing wall. This cross-flow component can be calculated by means of asymptotic theory and enabled Weinberg and Rubin[9] to derive a full set of self-similar equations governing the compressible corner flow problem using the formalism of matched asymptotic expansions. We take a different path and calculate the flow as a solution to the parabolized Navier-Stokes (PNS) equations. The two-dimensional stability of the incompressible limit was first examined by Parker and Balachandar[5] within the framework of temporal linear stability theory. Spatial stability was considered later by Galionis and Hall[3] by means of the parabolized stability equations (PSE). This paper intends to extend the linear stability analysis to the compressible flow regime. A representative supersonic free-stream Mach number of $Ma = 1.5$ is chosen for this purpose. The procedure used to obtain the laminar base flow is described in section II followed by the temporal linear stability analysis in section III. Conclusions are presented in section V.

II. Base flow

The laminar base flow is calculated as a solution to the parabolized Navier-Stokes equations with zero streamwise pressure gradient which can be written in compact matrix form as[7]

$$\mathsf{A}\frac{\partial \mathbf{q}}{\partial x} + \mathsf{B}\frac{\partial \mathbf{q}}{\partial y} + \mathsf{C}\frac{\partial \mathbf{q}}{\partial z} = 0. \tag{1}$$

Equation (1) is linearized by lagging of coefficients. The matrices A, B ,C are the coefficient matrices and $\mathbf{q} = [\rho, u, v, w, T]^T$ is the vector of primitive variables, namely, density ρ, Cartesian velocity components u, v, w and temperature T. The solution is spatially advanced in the streamwise direction from $\mathbf{q}^{(i)}$ to $\mathbf{q}^{(i+1)}$ over an integration step Δx using the implicit Euler method starting from the initial solution vector $\mathbf{q}^0 = [\rho_\infty, u_\infty, 0, 0, T_\infty]$ at $x = 0$. For the transversal planes, a pseudo-spectral Chebyshev-Chebyshev collocation method is used to calculate derivatives in the spanwise directions.[2] Thus, derivatives in the y and z-direction are obtained by multiplying the solution vector with the corresponding Chebyshev differentiation matrices $\mathsf{D_y}$ and $\mathsf{D_z}$. Additionally, a sponge zone enforces the asymptotic cross-flow profile near the far-field boundaries through a source term $\boldsymbol{\sigma}(\mathbf{q}^{(i+1)} - \mathbf{q}_r)$ in the momentum equations.[1] $\boldsymbol{\sigma}$ is a weight function and $\mathbf{q}_r$ the asymptotic cross flow solution calculated as suggested by.[4] The resulting discretized differential equation reads

$$\mathsf{A}\left(\frac{\mathbf{q}^{(i+1)} - \mathbf{q}^{(i)}}{\Delta x} + \mathrm{O}(\Delta x)\right) + \mathsf{B}\mathsf{D_y}\mathbf{q}^{(i+1)} + \mathsf{C}\mathsf{D_z}\mathbf{q}^{(i+1)} - \boldsymbol{\sigma}(\mathbf{q}^{(i+1)} - \mathbf{q}_r) = 0 \tag{2}$$

and can be recast as a linear system

$$\mathsf{L}\mathbf{q}^{(i+1)} = \mathbf{r}. \tag{3}$$

Equation (3) is solved on a transformed Gauss-Lobatto grid

$$y = a\frac{1+\hat{y}}{b-\hat{y}}, \quad a = \frac{y_i y_{max}}{y_{max} - 2y_i}, \quad b = 1 + \frac{2a}{y_{max}} \tag{4}$$

for the transversal planes. By means of transformation (4), the original Gauss-Lobatto points $\hat{y}_j = \hat{z}_j = \cos(j\pi/N)$, $j = 1, 2, \ldots N$ defined on $[-1, 1]$ are transformed to the physical space $[0, y_{max}]$ with half of the grid points concentrated on the interval $[0, y_i]$.[6] All length scales are non-dimensionalized by the local displacement thickness δ_1, pressure by twice the dynamic pressure $\rho_\infty u_\infty^2$ and all other quantities by their respective free-stream values. Subscript ∞ refers to free-stream values. We chose the incompressible definition $\delta_1 = \int_0^\infty \left(1 - \frac{u}{u_\infty}\right) dy$ of the momentum loss thickness. The state of the flow is described by the dimensionless Reynolds, Prandtl and Mach number

$$Re_x = \frac{\rho_\infty u_\infty x}{\mu_\infty}, \quad Pr = \frac{c_p \mu_\infty}{k_\infty}, \quad Ma = \frac{u_\infty}{a_\infty}. \tag{5}$$

Here, μ is the dynamic viscosity, c_p the heat capacity at constant pressure, k the thermal conductivity and a the speed of sound. The system of equations is closed by the assumption of an ideal gas governed by the equation of state

$$p = \rho R T. \tag{6}$$

with R denoting the ideal gas constant.The viscosity and thermal conductivity are determined as a function of the local temperature from Sutherland's law. We chose the following gas properties

$$\begin{gathered} Ma = 1.5, \quad Pr = 0.714, \\ p_\infty = 1.01325 \cdot 10^5 \,\mathrm{Pa}, \quad T_\infty = 293.15 \,\mathrm{K}, \\ \kappa = 1.4, \quad c_p = 1005 \,\tfrac{\mathrm{J}}{\mathrm{kg\,K}}, \quad R = 287 \,\tfrac{\mathrm{J}}{\mathrm{kg\,K}}, \end{gathered} \tag{7}$$

for our calculations. Here, $\kappa = c_p/c_v$ is the heat capacity ratio and c_v the heat capacity at constant volume. An adiabatic wall is assumed for temperature and density. No-slip conditions are enforced for the velocity components. A homogeneous Neumann, i.e. zero-gradient condition is applied to the solution vector on far-field boundaries. The solution is marched in space with steps of size $\Delta x = 0.00015$ from the initial solution vector $\mathbf{q}_0 = [\rho_\infty, u_\infty, 0, 0, T_\infty]$ on a 40×40 collocation point grid with $y_{max} = 45$ and $y_i = y_{max}/25$. Figure 2 shows a comparison between the PNS method at hand at an exemplary Reynolds number and the self-similar solution by Weinberg and Rubin[9] for three different Mach numbers. It can be seen that the streamwise (a) and crossflow (b) velocity profiles are in good agreement. The combined displacement effects of the two walls result in a jet-like crossflow profile as visualized in (c) by isolines of v.

III. Linear stability

Within the framework of temporal linear stability theory, the flow field is decomposed into a time dependent fluctuation $\mathbf{q}'$ and a steady primary state $\mathbf{q}_0$

$$\mathbf{q}(x, y, z, t) = \mathbf{q}_0(x, y, z) + \mathbf{q}'(x, y, z, t). \tag{8}$$

The steady primary state is given by the PNS solution in section II. The perturbation is assumed to be of normal mode form

$$\mathbf{q}'(x, y, z, t) = \hat{\mathbf{q}}(y, z) \cdot e^{\imath(\alpha x - \omega t)}. \tag{9}$$

Here, α is the streamwise wave number and ω is the angular frequency. Temporal growth of infinitesimally small disturbances occurs for imaginary parts of the angular frequency $\omega_i > 0$. Under the assumption of equations (8), (9) and a parallel base flow, the generalized eigenvalue problem of linear stability theory

$$\mathcal{A}\hat{\mathbf{q}} = \omega \mathcal{B}\hat{\mathbf{q}} \tag{10}$$

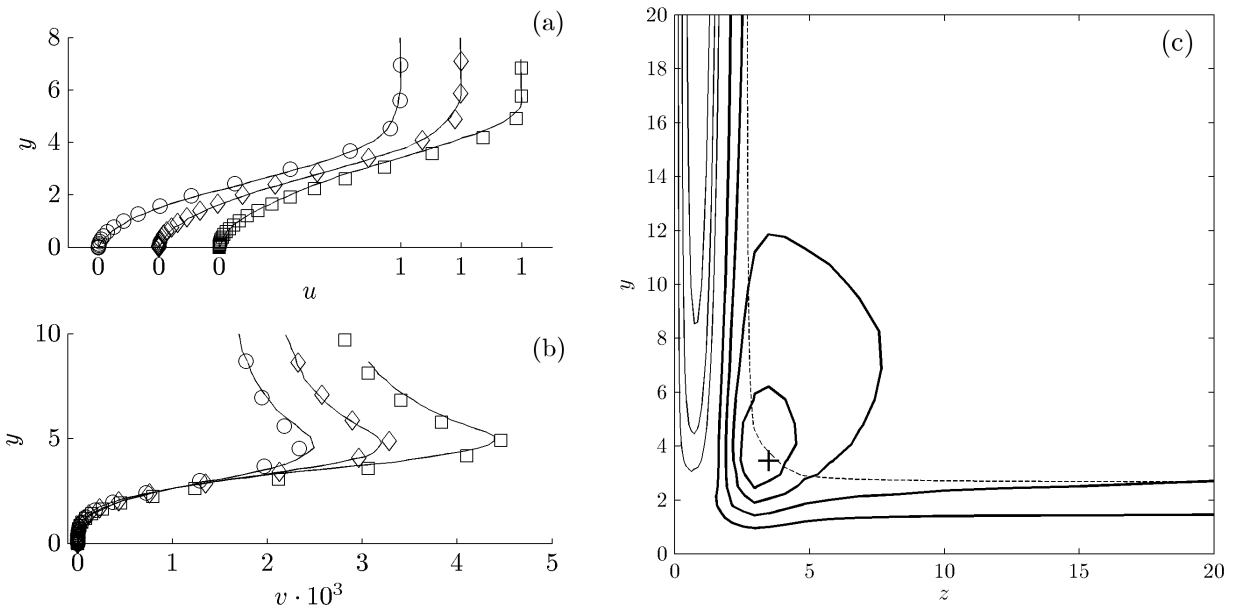

Figure 2. (a,b) Velocity profiles along symmetry line: (lines) self-similar solution of Weinberg & Rubin,[9] (∘) PNS for $Ma = 0.01$, (◇) PNS for $Ma = 0.95$, (□) PNS for $Ma = 1.5$; (a) streamwise velocity u, (b) crossflow velocity v. (c) Isolines of crossflow velocity v in the transversal plane at $Re_x = 5 \cdot 10^5$ and $Ma = 1.5$: (thick lines) $v > 0$, (thin lines) $v < 0$, (dashed line) $u = u_{99}$, (+) $v = v_{max}$.

is deduced from the Navier-Stokes equations. More details on two-dimensional linear stability theory can be found in Ref 8. At solid walls, zero velocity and temperature fluctuations are assumed

$$\hat{u} = \hat{v} = \hat{w} = \hat{T} = 0. \tag{11}$$

Sommerfeld's radiation condition

$$\frac{\partial \hat{\mathbf{q}}}{\partial n} = \imath\beta\hat{\mathbf{q}} \tag{12}$$

permits imposition of a phase angle $\tan^{-1}(\beta/\alpha)$ on far-field boundaries.[5] Figure 3 compares the spectra for a high resolution 65×65 grid with a lower resolution grid of 45×45 collocation points. It can be seen that the latter yields comparably good results in the relevant part of the spectrum (dashed box) with the grid clustering parameter y_i properly chosen. The dashed box encloses the most amplified modes of the Tollmien-Schlichting (TS) branch at phase speeds $c \approx 0.5$ and the inviscid corner modes (see section IV). The otherwise continuous branch is rendered discrete by the spacial discretization and the finite domain extend that allow only for modes of certain spanwise wave numbers to be resolved.

IV. Results

The linear stability problem (10) is solved for $Re_x = 8.9 \cdot 10^4$ corresponding to the critical Reynolds number of the one-dimensional asymptotic far-field profile at $\beta = 0$. The spanwise wave numbers resolved in the computational domain are not known a priori due to the break of symmetry by the corner. Therefore, we calculate solutions for a range of β enforced on far-field boundaries by means of Sommerfeld's radiation condition. Figure 4(a) shows part of the spectrum with pairs of even (-E) and odd-symmetric (-O) modes connected by dashed lines. Symmetric refers to symmetry with respect to the corner bisector. Latin numbers indicate multiples of the fundamental spanwise wave number. In addition to the viscous modes, a pair of inviscid corner modes (-C) can be seen. The odd-symmetric corner mode at $\omega_i \approx 0.25$ was not observed up to the present in incompressible corner flow stability studies. The dependence of the temporal amplification rate on β is depicted in 4(b). It can be seen that all modes but mode II-E experience maximum amplification at some negative value of β, i.e. incoming waves. The odd-symmetric corner mode shows almost no dependence on β as expected while its even-symmetric counterpart exhibits a small increase in temporal amplification around $\omega_i \approx -0.05$.

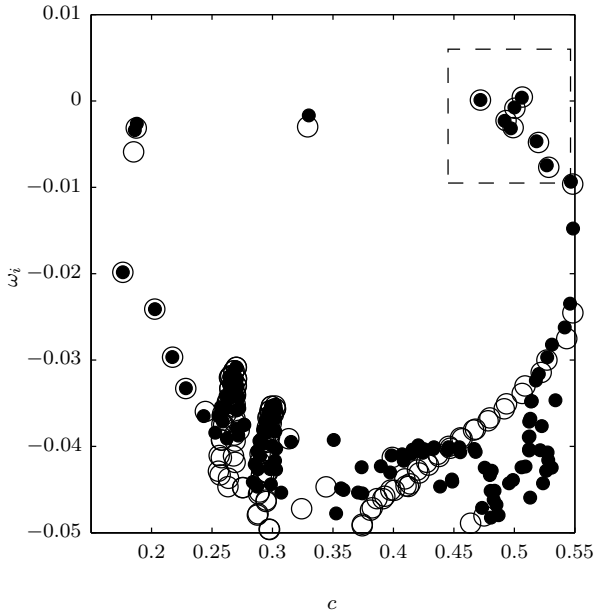

Figure 3. Convergence of eigenvalues for $Re_x = 2.5 \cdot 10^5$, $Ma = 1.5$, $\alpha = 0.2$, $\beta = 0$: (○) $N = 65$, $y_i = 2$, (•) $N = 45$, $y_i = y_{max}/5$, (dashed box) relevant part of spectrum.

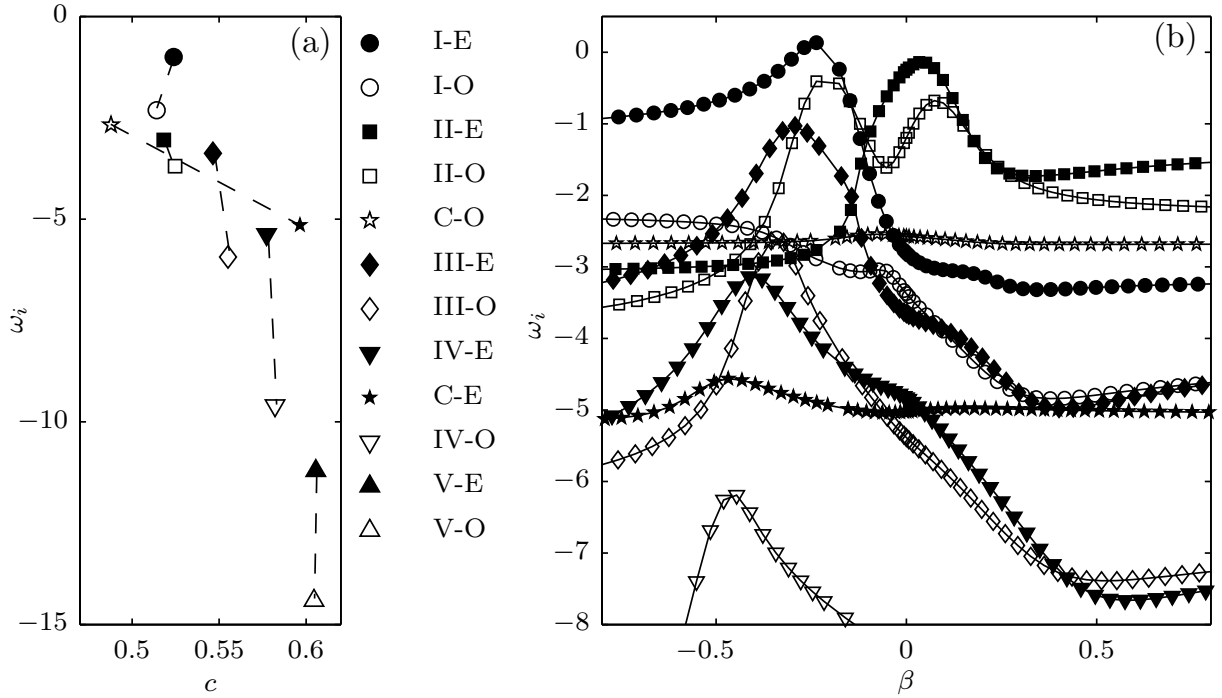

Figure 4. Dependence of temporal amplification on β for $Ma = 1.5$, $\alpha = 0.19$ at the critical Reynolds number of the one-dimensional far-field; (solid symbols, -E) even/symmetric TS modes, (empty symbols, -O) odd/antisymmetric TS modes, Latin numbers indicate increasing spanwise wave numbers, (dashed lines) connect even/odd mode pairs of equal spanwise wave number, (★, C) corner mode: (a) spectrum, (b) modal growth rates ω_i versus spanwise wave number β.

This viscous behavior of mode C-E is further investigated by visualizations of the eigenfield structure in figure 5. Isolines of the streamwise perturbation velocity $\hat{u}$ are shown in (a), a spatial-temporal reconstruction of the eigenfield is shown in (b) and a near-wall cutting plane of the latter at $y = 1$ in (c). It is observed that the mode changes its form towards a modulated structure typical for higher harmonic TS type instabilities at some distance from the corner ($y, z \gtrsim 15$).

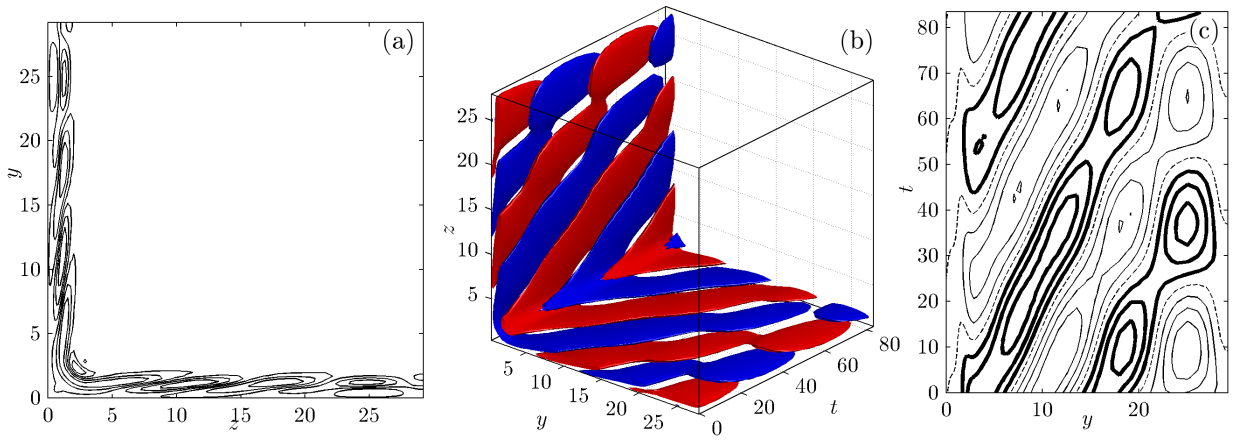

Figure 5. Eigenfield of streamwise perturbation velocity $\hat{u}$ for the even-symmetric corner mode (C-E) at $Re_x = 8.9 \cdot 10^4$, $Ma = 1.5$, $\alpha = 0.19$, $\beta = -0.21$: (a) contours of $|\hat{u}|$, (b) temporal isosurfaces (blue: $\hat{u} = -0.75\hat{u}_{max}$, red: $\hat{u} = 0.75\hat{u}_{max}$), (c) Temporal evolution of streamwise perturbation velocity contours over 1.5 periods at constant wall distance $z = 1$; (thick lines) $\hat{u} > 0$, (thin lines) $\hat{u} < 0$, (dashed line) $\hat{u} = 0$.

The odd-symmetric corner mode as shown in figure 6 is spatially restricted to the corner region and possesses a higher temporal growth rate. However, both modes are damped for the Reynolds number investigated.

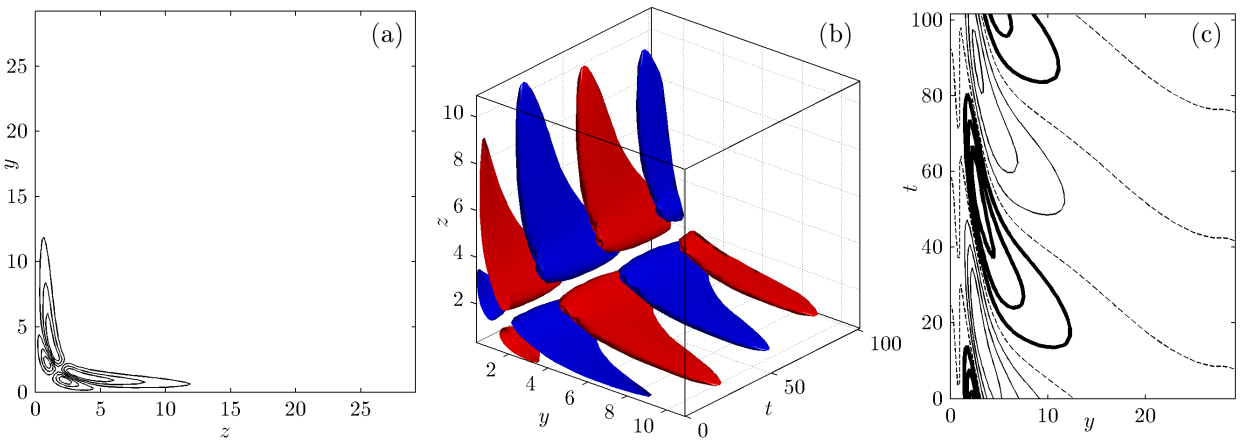

Figure 6. Same as Figure 5 for the odd-symmetric corner mode (C-O).

In a next step, the computational domain is spatially extended for proper resolution of acoustic modes. This is done by extrapolation of the PNS base flow solution from $y_{max} = 45$ to $y_{max} = 80$ under the assumption of a constant far-field solution comprised of the asymptotic limit for all flow quantities. Additionally, the number of collocation points along each direction is increased to $N = 60$ to obtain converged results. A spectrum for the enlarged domain calculation is depicted in figure 7. The most distinct features of the spectrum are the continuous branch at $c \approx 1$, the fundamental and two higher harmonic TS branches and the horizontally aligned fast (right, $c \gtrsim 1.66$) and slow (left, $c \lesssim 0.33$) traveling acoustic mode branches. Note that all acoustic modes are temporally dampened as in the flat-plate scenario.

The acoustic modes can be categorized with respect to speed (fast and slow, $c = 1 \pm 1/Ma$), symmetry and wall-boundedness. Examples of each are presented in figure 8. While modes (a-c) are active in the far-field, modes (d) and (e) appear wall-bounded. Among higher harmonics of wall-bounded and non-wall-bounded modes an acoustic corner mode is identified in the slowly traveling branch (f, note the different coordinate

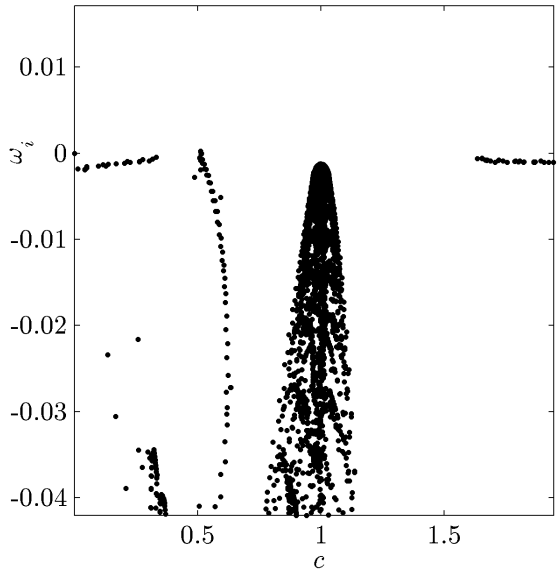

Figure 7. Eigenvalue spectrum for $Re_x = 8.9 \cdot 10^4$, $Ma = 1.5$, $\alpha = 0.19$, $\beta = 0$, $N = 60$, $y_i = y_{max}/8$, $y_{max} = 80$.

scaling).

V. Conclusions

The linear stability of the flow in a streamwise corner is studied at $Ma = 1.5$ and $Re_x = 9.8 \cdot 10^4$. Temporal growth rates of incoming and outgoing waves are obtained by variation of the far-field phase angle through Sommerfeld's radiation condition. A new inviscid, odd-symmetric corner mode is identified in the spectrum which was not observed in hitherto existing studies. Additionally, acoustic disturbances are calculated in an enlarged computational domain. Among them, an acoustic corner mode is found.

References

[1]D. J. Bodony. Analysis of sponge zones for computational fluid mechanics. *Journal of Computational Physics*, 212:681–702, March 2006.

[2]C. Canuto, M.Y. Hussaini, A. Quarteroni, and T.A. Zang. *Spectral methods in fluid dynamics*. Springer New York, 1988.

[3]I. Galionis and P. Hall. Spatial stability of the incompressible corner flow. *Theoretical and Computational Fluid Dynamics*, 19:77–113, May 2005.

[4]K. N. Ghia and R. T. Davis. A Study of Compressible Potential and Asymptotic Viscous Flows for Corner Region. *AIAA Journal*, 12:355–359, March 1974.

[5]S. J. Parker and S. Balachandar. Viscous and Inviscid Instabilities of Flow Along a Streamwise Corner. *Theoretical and Computational Fluid Dynamics*, 13:231–270, 1999.

[6]P.J. Schmid and D.S. Henningson. *Stability and transition in shear flows*. Springer Verlag, 2001.

[7]J. Tannehill, D. Anderson, and R. Pletcher. *Computational Fluid Mechanics and Heat Transfer*. Taylor & Francis, 1997.

[8]V. Theofilis. Advances in global linear instability analysis of nonparallel and three-dimensional flows. *Progress in Aerospace Sciences*, 39:249–315, May 2003.

[9]B. C. Weinberg and S. G. Rubin. Compressible corner flow. *Journal of Fluid Mechanics*, 56:753–774, 1972.

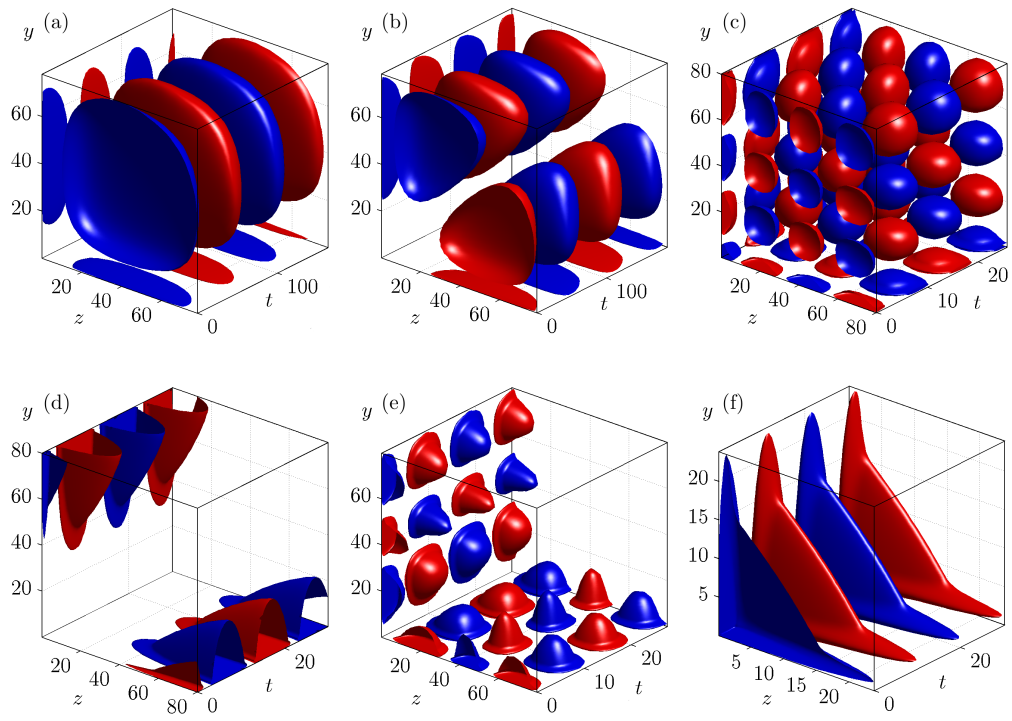

Figure 8. Isosurfaces of the streamwise perturbation velocity $\hat{u}$ for $Re_x = 8.9 \cdot 10^4$, $Ma = 1.5$, $\alpha = 0.19$, $\beta = 0$, $N = 60$, $y_i = {}^{y_{max}}/_{8}$, $y_{max} = 80$ (blue: $\hat{u} = -0.75\hat{u}_{max}$, red: $\hat{u} = 0.75\hat{u}_{max}$): (a) even fast acoustic mode, (b) odd fast acoustic mode, (c) even slow acoustic mode, (d) fundamental and (e) higher harmonic wall-bounded slow acoustic modes, (e) slow even acoustic corner mode.